Title
Formation of energetic electron butterfly distributions by magnetosonic waves via Landau resonance

Journal
GEOPHYSICAL RESEARCH LETTERS, 43(7)

ISSN
0094-8276

Authors
Li, Jinxing
Ni, Binbin
Ma, Qianli
et al.

Publication Date
2016

DOI
10.1002/2016GL067853

Peer reviewed

AGU PUBLICATIONS

Geophysical Research Letters

RESEARCH LETTER
10.1002/2016GL067853

Key Points:
- Electron butterfly distributions of ~100 keV are quickly formed in the radiation belts
- Electron butterfly distributions are observed in direct association with magnetosonic waves
- Numerical simulations produce butterfly distributions similar to the observations

Supporting Information:
- Supporting Information S1

Correspondence to:
B. Ni and L. Xie,
bbni@whu.edu.cn;
xielun@pku.edu.cn

Citation:
Li, J., et al. (2016), Formation of energetic electron butterfly distributions by magnetosonic waves via Landau resonance, *Geophys. Res. Lett.*, *43*, 3009–3016, doi:10.1002/2016GL067853.

Received 18 JAN 2016
Accepted 27 FEB 2016
Accepted article online 6 MAR 2016
Published online 4 APR 2016

Formation of energetic electron butterfly distributions by magnetosonic waves via Landau resonance

Jinxing Li[1,2], Binbin Ni[3], Qianli Ma[2], Lun Xie[1], Zuyin Pu[1], Suiyan Fu[1], Richard M. Thorne[2], Jacob Bortnik[2], Lunjin Chen[4], Wen Li[2], Daniel N. Baker[5], Craig A. Kletzing[6], William S. Kurth[6], George B. Hospodarsky[6], Joseph F. Fennell[7], Geoffrey D. Reeves[8], Harlan E. Spence[9], Herbert O. Funsten[10], and Danny Summers[11]

[1]Institute of Space Physics and Applied Technology, Peking University, Beijing, China, [2]Department of Atmospheric and Oceanic Sciences, University of California, Los Angeles, California, USA, [3]Department of Space Physics, School of Electronic Information, Wuhan University, Wuhan, China, [4]W. B. Hanson Center for Space Sciences, Department of Physics, University of Texas at Dallas, Richardson, Texas, USA, [5]Laboratory for Atmospheric and Space Physics, University of Colorado Boulder, Boulder, Colorado, USA, [6]Department of Physics and Astronomy, University of Iowa, Iowa City, Iowa, USA, [7]Space Science Applications Laboratory, The Aerospace Corporation, El Segundo, California, USA, [8]Space Science and Applications Group, Los Alamos National Laboratory, Los Alamos, New Mexico, USA, [9]Each Institute for the Study of Earth, Oceans, and Space, University of New Hampshire, Durham, New Hampshire, USA, [10]Los Alamos National Laboratory, Los Alamos, New Mexico, USA, [11]Department of Mathematics and Statistics, Memorial University of Newfoundland, St. John's, Newfoundland, Canada

Abstract Radiation belt electrons can exhibit different types of pitch angle distributions in response to various magnetospheric processes. Butterfly distributions, characterized by flux minima at pitch angles around 90°, are broadly observed in both the outer and inner belts and the slot region. Butterfly distributions close to the outer magnetospheric boundary have been attributed to drift shell splitting and losses to the magnetopause. However, their occurrence in the inner belt and the slot region has hitherto not been resolved. By analyzing the particle and wave data collected by the Van Allen Probes during a geomagnetic storm, we combine test particle calculations and Fokker-Planck simulations to reveal that scattering by equatorial magnetosonic waves is a significant cause for the formation of energetic electron butterfly distributions in the inner magnetosphere. Another event shows that a large-amplitude magnetosonic wave in the outer belt can create electron butterfly distributions in just a few minutes.

1. Introduction

Earth's electron radiation belts are generally comprised of two distinct zones of trapped energetic electrons, separated by a "slot" region [*Allen and Frank*, 1959]. Temporal and spatial changes in Earth's radiation belts result from a delicate imbalance between various physical processes acting as sources and sinks [*Reeves et al.*, 2003]. The outer radiation belt that typically occupies $L = 3 - 8$ (where L is the equatorial radial distance of the dipole geomagnetic field in units of Earth radius) is highly dynamic and subject to change in response to geomagnetic activity mediated by interactions with a variety of magnetospheric waves [*Baker et al.*, 2004; *Horne et al.*, 2005; *Chen et al.*, 2007; *Summers et al.*, 2007; *Reeves et al.*, 2013; *Thorne et al.*, 2013]. While the inner belt and slot region are largely isolated from many magnetospheric processes, their dynamic responses to geomagnetic storms are clearly observed through variations in pitch angle and energy distributions [*Zhao et al.*, 2014a, 2014b; *Baker et al.*, 2013]. Radiation belt electrons undergo three periodic motions in the ambient geomagnetic field: gyration, bounce, and drift, each of which corresponds to an adiabatic invariant and a characteristic timescale. Violation of any of the adiabatic invariants can result in energy and pitch angle variations of electrons and corresponding changes in the electron distribution.

Dynamic variations of electron pitch angle distribution and their spectral dependence are important signatures of the underlying physical processes that act on these populations, since electrons of different pitch angles at different energies behave differently when subjected to external influences. In situ observations of radiation belt electrons demonstrate three commonly featured categories of electron pitch angle distributions: 90° peaked (or normal), flattop (or pancake), and butterfly [*West et al.*, 1973; *Meredith et al.*, 2000; *Gannon et al.*, 2007; *Gu et al.*, 2011; *Baker et al.*, 1978; *Fritz et al.*, 2003; *Horne et al.*, 2003; *Zhao et al.*, 2014a, 2014b]. Inward radial diffusion driven by ultralow frequency waves causes electron flux to increase near 90° faster than other pitch angles, thus creating a 90° peaked distribution or altering an apparent butterfly distribution at a higher L shell

into a flattop and eventually into a 90° peaked distribution at a lower L shell [*Ukhorskiy et al*., 2009]. Ninety degree peaked distributions can also be steepened due to energy diffusion by very low frequency chorus waves or pitch angle scattering loss by electromagnetic ion cyclotron waves [*Li et al*., 2007]. Scattering by extremely low frequency (ELF) plasmaspheric hiss acts as a dominant cause of pancake-shaped distributions in the inner magnetosphere [*Ni et al*., 2013].

Butterfly distributions, characterized by a local flux minimum near 90° pitch angle, are usually explained in terms of drift shell splitting and losses to the magnetopause due to the local time asymmetry in the geomagnetic field [*Fritz et al*., 2003; *Roederer*, 1970; *Selesnick and Blake*, 2002; *Turner et al*., 2012] and field line stretching [*Baker et al*., 1978], since equatorially mirroring electrons on the dayside drift out farther than those at other pitch angles, thereby enhancing their escape from the magnetosphere. This mechanism can account for the occurrence of butterfly distributions at high L shells close to the outer magnetospheric boundary. However, it fails to explain the persistent butterfly distributions in the inner belt [*Zhao et al*., 2014a, 2014b] where neither field distortion nor drift shell splitting is significant. While a process of nonlocal acceleration occurring at higher latitudes was proposed to possibly explain observations of butterfly distributions well below the outer magnetospheric boundary [*Horne et al*., 2003], that scenario has not been verified with either simulations or observations. The outstanding question as to what causes the peculiar and persistent butterfly distributions at lower L shells in the radiation belts remains unresolved.

This paper presents the Van Allen Probe observations during the 27–29 June 2013 geomagnetic storm. In this storm, the energetic electron butterfly distributions coexisted in the same region as magnetosonic waves. The initial 90° peaked distributions in the slot region quickly evolved into butterfly distributions after the magnetosonic wave intensification. Our numerical simulations produced a butterfly distribution formation process that is consistent with the observations, indicating that the electron butterfly distributions are caused by parallel acceleration due to Landau resonance with magnetosonic waves. Another event occurring on 21 August 2013 showed that a very large amplitude magnetosonic wave at $L = 4.7$ can create electron butterfly distributions in just a few minutes, which is also reproduced by our simulations.

2. Particle Evolution and Magnetosonic Wave Observations

A geomagnetic storm hit the earth on 27 June 2013 with a minimum *SYM-H* index reaching −110 nT as shown in Figure 1a. Figures 1c–1h present the electron pitch angle evolution at various energies measured by the Magnetic Electron Ion Spectrometer (MagEIS) [*Blake et al*., 2013] on board Van Allen Probe B [*Mauk et al*., 2013] at $L = 2.4$ over selected times represented by the solid lines in Figures 1a and 1b. We have transformed the particle local pitch angles to equatorial pitch angles by assuming a dipole geomagnetic field, which is fairly accurate in the inner magnetosphere. The initial pitch angle distributions for hundreds of keV electrons during the storm main phase were peaked at 90° (note that the measured 600 keV electron flux were near the noise level, and thus, this cannot be accurately determined) but evolved into butterfly distributions in about 10 h in association with intense magnetosonic waves. The low-energy (32 keV and 75 keV) electrons became flattop distributions before ~1253 UT and subsequently returned to 90° peaked distributions at 1420 UT, which may be caused by a substorm injection indicated by the *AE* index shown in Figure 1b and an inward radial diffusion process. The measurements of $>$ 600 keV electrons were below the threshold noise level of MagEIS and thus are not shown.

The dynamics of energetic electron differential fluxes is shown as a function of universal time and pitch angle in Figures 2a–2c, illustrating the development of electron butterfly distributions in the radial range from $L = 1.4$ in the inner belt to $L = 3.2$ in the outer belt. The observed evolution of energetic electron butterfly distributions in the slot region and inner belt is not a consequence of drift shell splitting or magnetopause shadowing that is insignificant at the inner magnetosphere below $L \sim 5$. However, from the wave power spectral density profile in the frequency range of 10 Hz–12 kHz measured by the waveform receiver (WFR) [*Kletzing et al*., 2013] on board the spacecraft (Figures 2g and 2h), a class of intense electromagnetic waves called fast magnetosonic (MS) waves, also known as "equatorial noise" [*Russell et al*., 1969; *Santolík et al*., 2002], was found to occur roughly in the same region and at the same time as the electron butterfly distributions. The magnetosonic waves were identified by their frequencies general between proton gyrofrequency (f_{cp}) and lower hybrid resonant frequency (f_{LHR}), ellipticity close to zero (Figure 2g), and wave normal angles close to 90° (Figure 2h). The harmonic structure [*Perraut et al*., 1982; *Santolík et al*., 2002; *Balikhin et al*., 2015] of those magnetosonic waves was almost

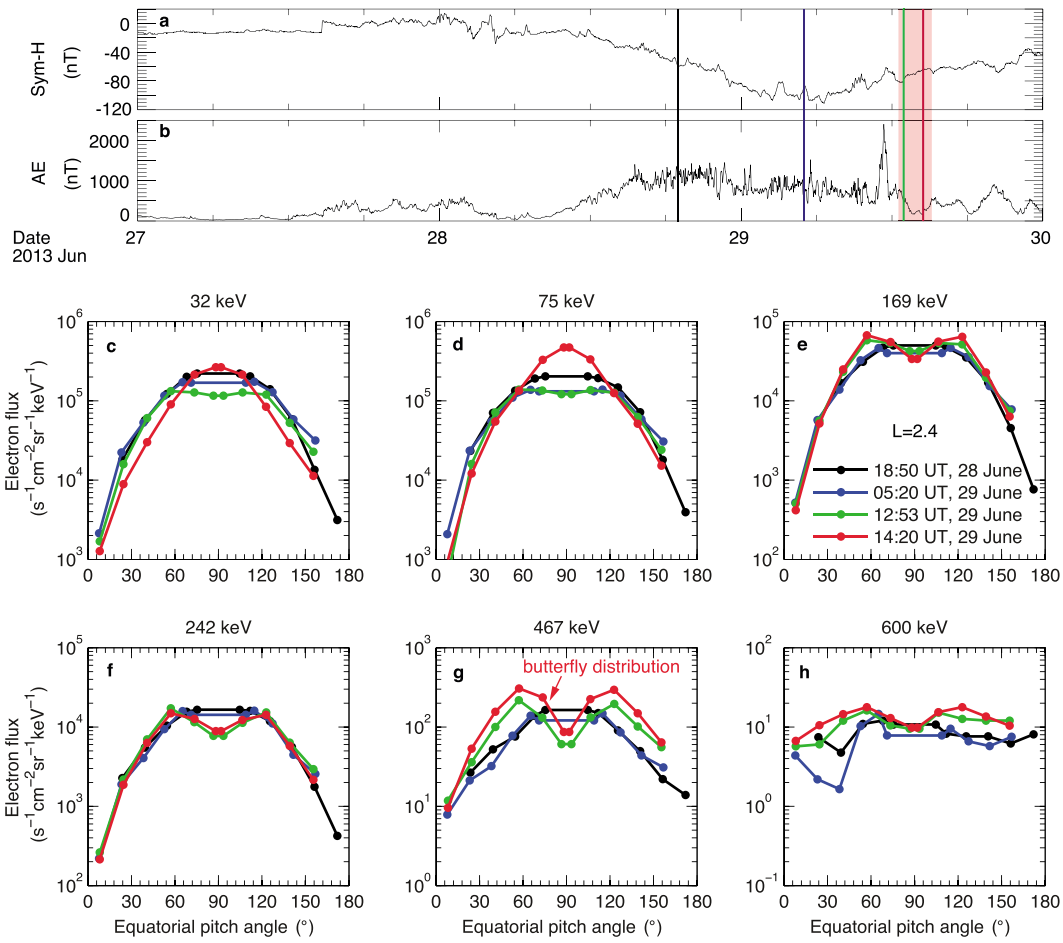

Figure 1. Geomagnetic indexes during the period of 27–29 June 2013 and electron differential flux evolution for the selected energies at $L = 2.4$ measured by MagEIS on board Van Allen Probe B. (a) Geomagnetic *SYM-H* index, which is a longitudinally symmetric (SYM) disturbance index describing the horizontal (H) component of geomagnetic disturbance fields at midlatitudes with 1 min resolution and (b) *AE* index which is a proxy of substorm injections. (c–h) Electron differential flux over selected times represented by solid lines in Figures 1a and 1b. The electron fluxes for the energy range of 32–600 keV initially exhibited 90° peaked pitch angle distributions during the storm main phase and evolved into clear butterfly distributions at 12:53 UT on 29 June during the recovery phase. The electron fluxes at 32 and 75 keV peaked at 90° again at 14:20 UT, possibly due to enhanced substorm injections indicated by the *AE* index.

identical along the orbit with a separation of 32 Hz, showing that these waves were generated from a localized source near $L = 2.5$ (the corresponding proton gyrofrequency ~ 32 Hz) and propagated into other locations in the inner magnetosphere (see supporting information for detailed discussions of the wave generation). Those magnetosonic waves were observed inside the plasmasphere over a wide magnetic local time (MLT) region and covered a radial range of $L = 1.2$–3.2 which was similar to that of the electron butterfly distributions. Although the electron butterfly distributions observed in $L = 2.8$–3.2 on the postmidnight side (12:30–12:45 UT) exceeded the upper altitude of magnetosonic waves, a possible explanation is that they might have drifted from the duskside where magnetosonic waves were indeed recorded during 14:30 and 14:40 UT (Figure 2). The Van Allen Probe A also recorded similar profiles of intense magnetosonic waves (Figure S4 in the supporting information). In addition, plasmaspheric hiss emissions with frequencies higher than that of magnetosonic waves were also recorded over a broad radial range but within a narrower MLT range. The spectral intensities of hiss waves were at least an order of magnitude smaller than those of magnetosonic waves.

3. Simulation of Butterfly Distribution Formation

In order to quantitatively examine the underlying impact of magnetosonic waves on the formation of electron butterfly distributions, an accurate magnetic and electric field model of broadband magnetosonic

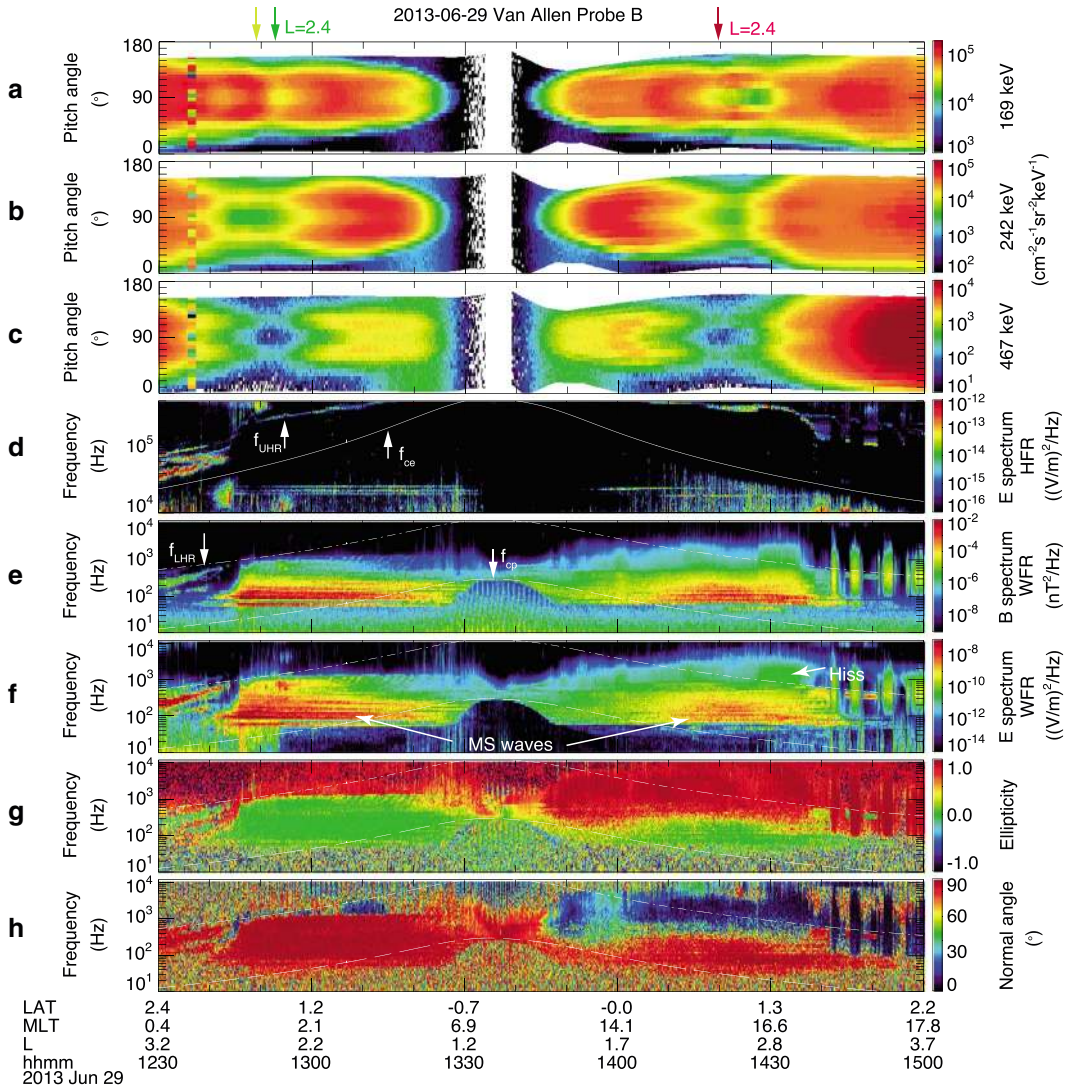

Figure 2. Electron differential flux and plasma wave observations by Van Allen Probe B during the interval of 12:30–15:00 UT on 29 June 2013. Differential fluxes of radiation belt energetic electrons measured by the MagEIS instrument ((a) 169 keV, (b) 242 keV, and (c) 467 keV) as a function of pitch angle. (d) High-frequency receiver (HFR) electric wave spectrum in the frequency range of 10–500 kHz, overplotted with the upper hybrid resonance frequency (f_{UHR}) and the electron gyrofrequency (f_{ce}). (e) Waveform receiver (WFR) magnetic wave spectrum in the frequency range of 10–12,000 Hz, overplotted with lower hybrid resonance frequency (f_{LHR}) and proton gyrofrequency (f_{cp}). (f) WFR electric wave spectrum corresponding to Figure 2e. (g) Wave ellipticity and (h) wave normal angle computed using the singular value decomposition method. Observations show an evident transition of 90° peaked distributions to butterfly distributions when the activity of fast magnetosonic waves was enhanced.

waves, based on the Van Allen Probes waveform data, is developed at a representative location near $L = 2.4$ (details are described in the supporting information) and then adopted for test particle simulations [*Li et al.*, 2014, 2015] to capture both contributions of the Landau resonance [*Horne et al.*, 2007; *Ni and Summers*, 2010] and transit time scattering [*Bortnik and Thorne*, 2010]. The obtained drift and bounce averaged rates of pitch angle diffusion, momentum diffusion, and cross diffusion (Figures 3a–3c) indicate that the observed magnetosonic waves could drive efficient pitch angle, momentum, and cross diffusion (on the timescale of hours) for electrons above several keV but predominantly confined to equatorial pitch angles above 60°, which is a key factor that modulates the distinct variations of the electron population at different pitch angles.

Using the test particle simulated scattering rates, we numerically solve the two-dimensional Fokker-Planck diffusion equation to simulate the temporal variations of energetic electrons including their pitch angle evolution.

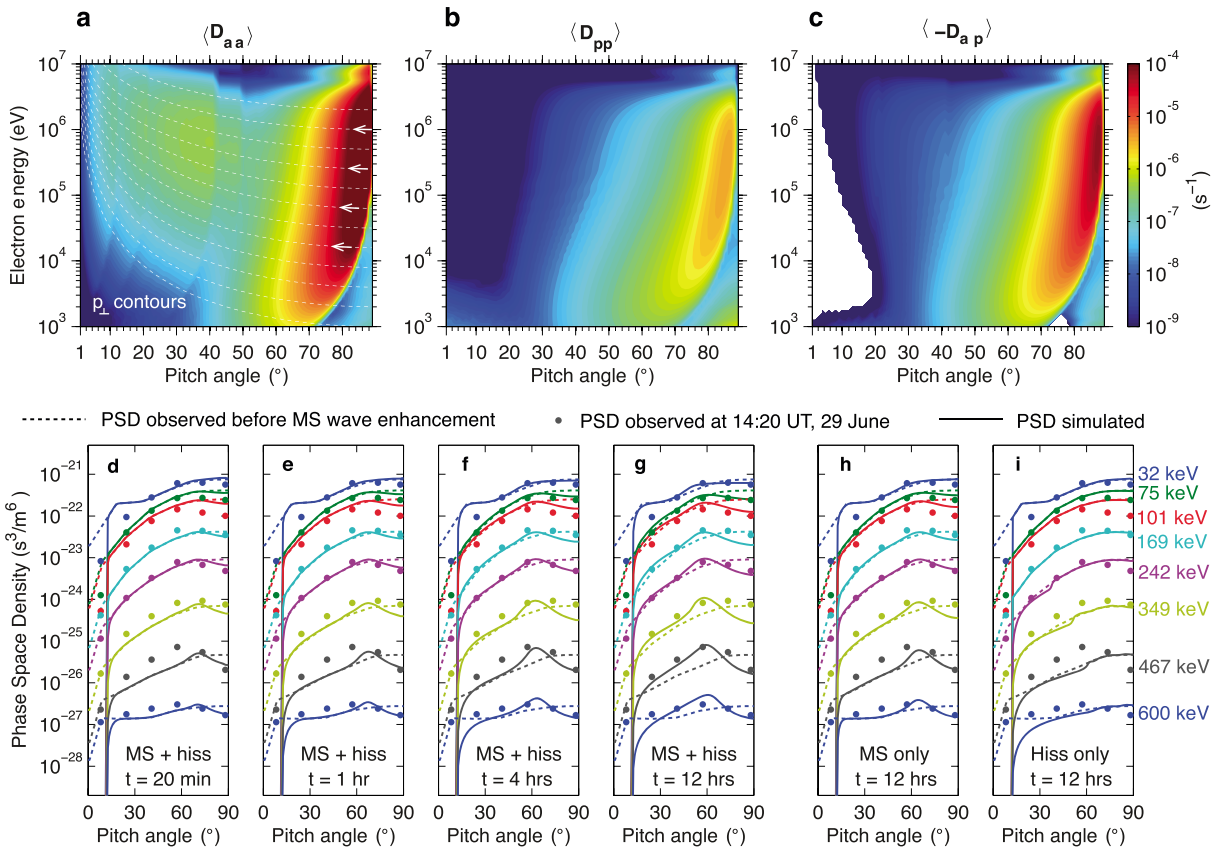

Figure 3. Computed diffusion coefficients for resonant interactions between fast magnetosonic waves and radiation belt electrons in the slot region and simulated electron phase space density (PSD) evolution at selected energies with comparisons to observations. (a–c) Test particle simulated drift- and bounce-averaged rates of pitch angle diffusion, momentum diffusion, and (pitch angle and momentum) mixed diffusion of interactions between fast magnetosonic waves and radiation belt electrons at $L = 2.4$, in which the white lines represent $p_\perp$ contours along which the Landau resonance should follow. (d–g) The temporal evolution of PSD under the combined impact of magnetosonic waves and hiss. (h) The simulated PSD variation under magnetosonic waves only. (i) The PSD variation under the impact of hiss only. The dashed line represents the initial electron PSD, and the stars represent the butterfly-shaped PSD observed at 14:20 UT on 29 June (except that the 32 and 75 keV channels were measured at 12:50 UT before the injections). The 90° pitch angle electrons are transported to low pitch angles under the impact of magnetosonic waves and hiss, while scattering by magnetosonic waves is primarily responsible for the formation of butterfly distributions.

The results (Figures 3d–3i) confirm that scattering by magnetosonic waves dominantly controls the formation of energetic electron butterfly distributions in the slot region. While the observed plasmaspheric hiss can play a role in diffusing energetic electrons into the loss cone, its scattering leads to flattop distributions (Figure 3i), and makes little contribution to the electron variations at pitch angles above 50°. Responding to interactions with magnetosonic waves, the energetic electrons near 90° pitch angle are transported gradually to 50°–70° pitch angles, thereby evolving from 90° peaked distributions to butterfly distributions within 20 min (Figure 3d). As the wave-particle interactions continue, the energetic electron butterfly pitch angle distributions deepen and agree well with the MagEIS observations (Figures 3e–3g), further supporting the dominance of magnetosonic wave scattering to the formation of energetic electron butterfly distributions in the slot region.

The occurrence of butterfly distributions is attributed to parallel acceleration through Landau resonant interactions with magnetosonic waves, which primarily change the parallel momentum of electrons [*Lyons and Williams*, 1984] and cause them to diffuse approximately along the perpendicular momentum contours. As a consequence, the negative cross diffusion rates by magnetosonic waves (Figure 3c) result in decreases in pitch angle when energetic electrons diffuse to higher energies along the gradient of phase space density. Furthermore, since the diffusion rates become significantly smaller at pitch angles lower than 60°, the electron population tends to drop at 90° pitch angle and pile up at 50°–60° pitch angles, therefore creating the characteristic butterfly distributions.

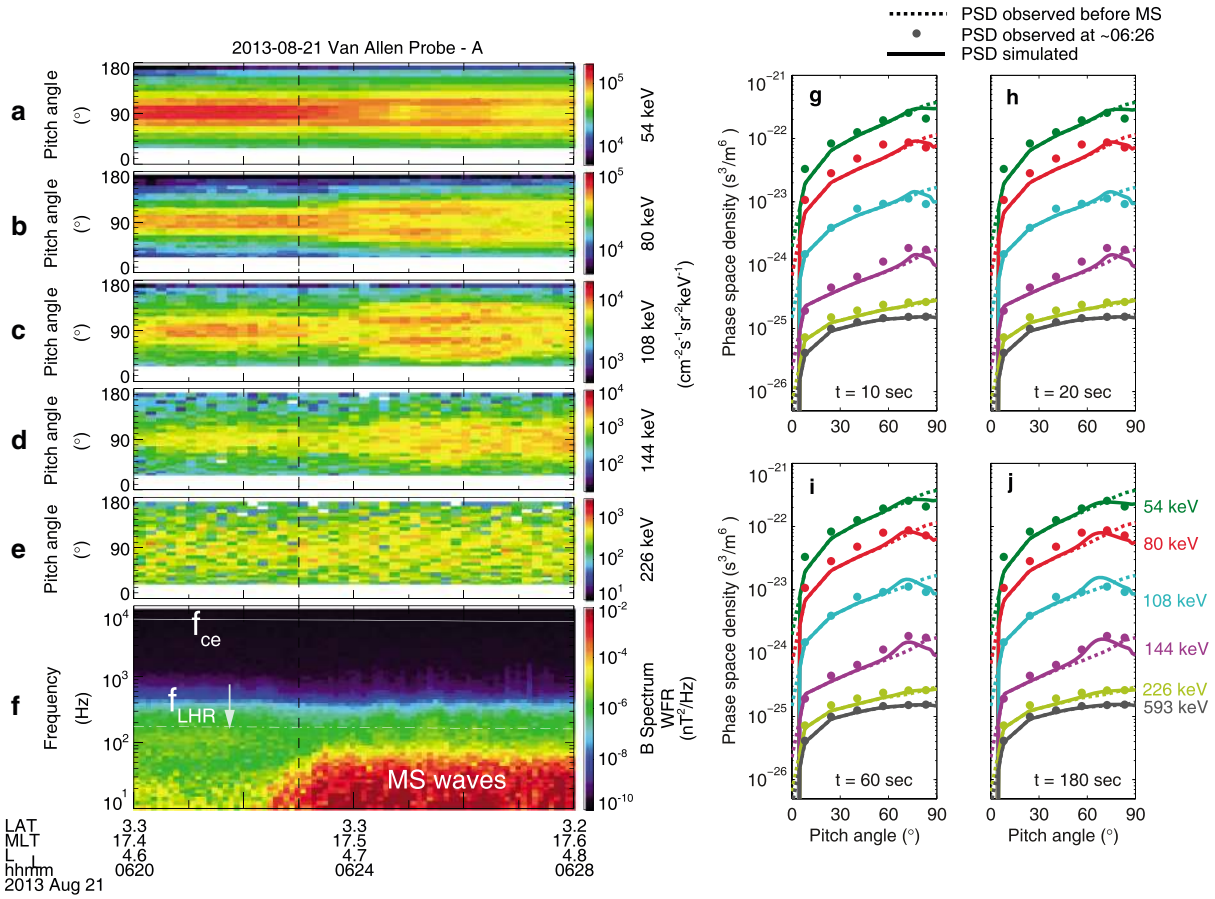

Figure 4. An observation and corresponding simulation of magnetosonic waves rapidly shaping the butterfly distributions of 54–144 keV electrons at $L \simeq 4.7$ in the outer radiation belt during the 21 August 2013 event. (a–e) The evolution of electron fluxes at 32–232 keV channels during an 8 min interval measured by MagEIS on board Van Allen Probe A. (f) The wave magnetic spectral intensity. (g–j) Simulated electron PSD evolution and comparisons to observations. The initial PSDs were 2 min averaged before the enhancement of magnetosonic waves, while the final PSDs were averaged within 2–4 min after the intensification of magnetosonic waves. The 54–144 keV electrons exhibited butterfly pitch angle distributions within 1 min after the arrival of intense magnetosonic waves, as shown from both observations and simulations.

4. Discussion

The electron butterfly distributions observed throughout the region $1.4 < L < 3.2$ can be explained by scattering due to equatorial magnetosonic waves located in the same spatial region for the above event. Equatorial magnetosonic waves can also rapidly modulate electrons in the outer radiation belt as far as $L = 4.7$ from 90° peaked distributions to butterfly distributions, as illustrated in Figure 4 for the 21 August 2013 event. The electrons measured by MagEIS on board Van Allen Probe A initially exhibited 90° peaked distributions (Figures 4a–4e). When an extremely intense magnetosonic wave (~1.5 nT) appeared at 06:23 UT (Figure 4f), the population of 54–144 keV electrons evolved into butterfly distributions within 1 min, while the higher-energy electrons did not (Figure 4e). The butterfly distributions are formed much faster in this case than that in the 29 June 2013 event because the wave intensity was 9 times larger, while the background magnetic field strength was approximately 1/8 of that in the previous event. Our simulation of the dynamic response of outer zone energetic electrons to magnetosonic wave scattering (Figures 4g–4j) is able to reproduce both the temporally prompt formation of butterfly distributions and its strong dependence on electron kinetic energy.

5. Conclusions

Our results demonstrate definitively that scattering by equatorial magnetosonic waves provides an efficient mechanism for energetic electron diffusion in the slot region and outer belt and can primarily account for the formation of butterfly distributions at lower L shells in the inner magnetosphere. This conclusion is distinct

from previous theoretical studies [*Horne et al*., 2007] which concluded that magnetosonic waves are capable of locally accelerating electrons based on the acceleration timescales but did not simulate the change in pitch angle distribution due to parallel acceleration during Landau resonance. It is also different from the study by *Xiao et al*. [2015], in which the combined effect of chorus and magnetosonic waves accelerate the 30°–60° electrons faster than other pitch angle ones and created butterfly distributions at higher L shells ($L \simeq 4.8$). Since equatorial magnetosonic waves are ubiquitous in Earth's magnetosphere [*Ma et al*., 2013], our results also highlight the importance of magnetosonic waves to future comprehensive simulations of radiation belt electron dynamics and analyses of resonant wave-particle interactions in the inner magnetosphere.

Acknowledgments
This work was funded by the NSFC grants 41374166, 41274167, 41204120, and 41474141 and by the Chinese Key Research Project 2011CB811404. This work was also supported by JHU/APL contracts 967399 and 921647 under NASA's prime contract NAS5-01072. The analysis at UCLA was supported by the EMFISIS subaward 1001057397:01, the ECT subaward 13-041, the NASA grants NASA NNX13AI61G and NNX14AN85G, and NSF Geospace Environment Modeling grant AGS-1103064. D.S. acknowledges support from a Discovery Grant of the Nature Science and Engineering Research Council of Canada. We thank J. Bernard Blake and Seth G. Claudepierre for providing the Van Allen Probes MagEIS data and the World Data Center for Geomagnetism, Kyoto, for providing *SYM-H* and *AE* indices used in this study. The MagEIS data were downloaded from Van Allen Probe ECT website at http://www.rbsp-ect.lanl.gov/, and the wave measurements were downloaded from EMFISIS website at http://emfisis.physics.uiowa.edu/. The THEMIS data were available from http://themis.ssl.berkeley.edu/data/themis/.

References

Allen, J. A., and L. A. Frank (1959), Radiation around the Earth to a radial distance of 107,400 km, *Nature*, *183*, 430–434, doi:10.1038/183430a0.
Baker, D. N., P. R. Higbie, E. W. Hones, and R. D. Belian (1978), High-resolution energetic particle measurements at 6.6 R_E, *J. Geophys. Res.*, *83*, 4863–4868, doi:10.1029/JA083iA10p04863.
Baker, D. N., S. G. Kanekal, X. Li, S. P. Monk, J. Goldstein, and J. L. Burch (2004), An extreme distortion of the Van Allen belt arising from the 'Hallowe'en' solar storm in 2003, *Nature*, *432*, 878–881, doi:10.1038/nature03116.
Baker, D. N., et al. (2013), A long-lived relativistic electron storage ring embedded in Earth's outer Van Allen belt, *Science*, *340*, 186–190, doi:10.1126/science.1233518.
Balikhin, M. A., Y. Y. Shprits, S. N. Walker, L. Chen, N. Cornilleau-Wehrlin, I. Dandouras, O. Santolik, C. Carr, K. H. Yearby, and B. Weiss (2015), Observations of discrete harmonics emerging from equatorial noise, *Nat. Commun.*, *6*, 7703, doi:10.1038/ncomms8703.
Blake, J., et al. (2013), The magnetic electron ion spectrometer (MagEIS) instruments aboard the radiation belt storm probes (RBSP) spacecraft, *Space Sci. Rev.*, *179*, 383–421, doi:10.1007/s11214-013-9991-8.
Bortnik, J., and R. M. Thorne (2010), Transit time scattering of energetic electrons due to equatorially confined magnetosonic waves, *J. Geophys. Res.*, *115*, A07213, doi:10.1029/2010JA015283.
Chen, Y., G. D. Reeves, and R. H. W. Friedel (2007), The energization of relativistic electrons in the outer Van Allen belt, *Nat. Phys.*, *3*, 614–617, doi:10.1038/nphys655.
Fritz, T. A., M. Alothman, J. Bhattacharjya, D. L. Matthews, and L. Chen (2003), Butterfly pitch angle distributions observed by ISEE-1, *Planet. Space Sci.*, *51*, 205–219, doi:10.1016/S0032-0633(02)00202-7.
Gannon, J. L., X. Li, and D. Heynderickx (2007), Pitch angle distribution analysis of radiation belt electrons based on Combined Release and Radiation Effects Satellite Medium Electrons A data, *J. Geophys. Res.*, *112*, A05212, doi:10.1029/2005JA011565.
Gu, X., Z. Zhao, B. Ni, Y. Y. Shprits, and C. Zhou (2011), Statistical analysis of pitch angle distribution of radiation belt energetic electrons near the geostationary orbit: CRRES observations, *J. Geophys. Res.*, *116*, A01208, doi:10.1029/2010JA016052.
Horne, R. B., N. P. Meredith, R. M. Thorne, D. Heynderickx, R. H. A. Iles, and R. R. Anderson (2003), Evolution of energetic electron pitch angle distributions during storm time electron acceleration to megaelectronvolt energies, *J. Geophys. Res.*, *108*(A1), 1016, doi:10.1029/2001JA009165.
Horne, R. B., et al. (2005), Wave acceleration of electrons in the Van Allen radiation belts, *Nature*, *437*, 227–230, doi:10.1038/nature03939.
Horne, R. B., R. M. Thorne, S. A. Glauert, N. P. Meredith, D. Pokhotelov, and O. Santolik (2007), Electron acceleration in the Van Allen radiation belts by fast magnetosonic waves, *Geophys. Res. Lett.*, *34*, L17107, doi:10.1029/2007GL030267.
Kletzing, C., et al. (2013), The electric and magnetic field instrument suite and integrated science (EMFISIS) on RBSP, *Space Sci. Rev.*, *179*, 127–181, doi:10.1007/s11214-013-9993-6.
Li, J., et al. (2014), Interactions between magnetosonic waves and radiation belt electrons: Comparisons of quasi-linear calculations with test particle simulations, *Geophys. Res. Lett.*, *41*, 4828–4834, doi:10.1002/2014GL060461.
Li, J., et al. (2015), Comparison of formulas for resonant interactions between energetic electrons and oblique whistler-mode waves, *Phys. Plasmas*, *22*, 052922, doi:10.1063/1.4914852.
Li, W., Y. Y. Shprits, and R. M. Thorne (2007), Dynamic evolution of energetic outer zone electrons due to wave-particle interactions during storms, *J. Geophys. Res.*, *112*, A10220, doi:10.1029/2007JA012368.
Lyons, L. R., and D. J. Williams (1984), *Quantitative Aspects of Magnetospheric Physics*, D. Reidel Co., Dordrecht, Netherlands.
Ma, Q., W. Li, R. M. Thorne, and V. Angelopoulos (2013), Global distribution of equatorial magnetosonic waves observed by THEMIS, *Geophys. Res. Lett.*, *40*, 1859–1901, doi:10.1002/grl.50434.
Mauk, B. H., N. J. Fox, S. G. Kanekal, R. L. Kessel, D. G. Sibeck, and A. Ukhorskiy (2013), Science objectives and rationale for the radiation belt storm probes mission, *Space Sci. Rev.*, *179*, 3–27, doi:10.1007/s11214-012-9908-y.
Meredith, N. P., R. B. Horne, A. D. Johnstone, and R. R. Anderson (2000), The temporal evolution of electron distributions and associated wave activity following substorm injections in the inner magnetosphere, *J. Geophys. Res.*, *105*, 12,907–12,917, doi:10.1029/2000JA900010.
Ni, B., and D. Summers (2010), Resonance zones for electron interactions with plasma waves in the Earth's magnetosphere: II. Evaluation for oblique chorus, hiss, EMIC and magnetosonic waves, *Phys. Plasmas*, *17*, 042903, doi:10.1063/1.3310835.
Ni, B., J. Bortnik, R. M. Thorne, Q. Ma, and L. Chen (2013), Resonant scattering and resultant pitch angle evolution of relativistic electrons by plasmaspheric hiss, *J. Geophys. Res. Space Physics*, *118*, 7740–7751, doi:10.1002/2013JA019260.
Perraut, S., A. Roux, P. Robert, and R. Gendrin (1982), A systematic study of ULF waves above F H+ from GEOS 1 and 2 measurements and their relationships with proton ring distributions", *J. Geophys. Res.*, *87*, 6219–6236, doi:10.1029/JA087iA08p06219.
Reeves, G. D., K. L. McAdams, R. H. W. Friedel, and T. P. O'Brien (2003), Acceleration and loss of relativistic electrons during geomagnetic storms, *Geophys. Res. Lett.*, *30*(10), 1529, doi:10.1029/2002GL016513.
Reeves, G. D., et al. (2013), Electron acceleration in the heart of the Van Allen radiation belts, *Science*, *341*, 991–994, doi:10.1126/science.1237743.
Roederer, J. G. (1970), *Dynamics of Magnetically Trapped Particles*, Springer, Berlin.
Russell, C. T., R. E. Holzer, and E. J. Smith (1969), Ogo 3 observations of elf noise in the magnetosphere: 1. Spatial extent and frequency of occurrence, *J. Geophys. Res.*, *74*, 755–777, doi:10.1029/JA074i003p00755.
Santolík, O., J. S. Pickett, D. A. Gurnett, M. Maksimovic, and N. Cornilleau-Wehrlin (2002), Spatiotemporal variability and propagation of equatorial noise observed by Cluster, *J. Geophys. Res.*, *107*(A12), 1495, doi:10.1029/2001JA009159.
Selesnick, R. S., and J. B. Blake (2002), Relativistic electron drift shell splitting, *J. Geophys. Res.*, *107*(A9), 1265, doi:10.1029/2001JA009179.

Summers, D., B. Ni, and N. P. Meredith (2007), Timescales for radiation belt electron acceleration and loss due to resonant wave-particle interactions: 2. Evaluation for VLF chorus, ELF hiss, and electromagnetic ion cyclotron waves, *J. Geophys. Res.*, *112*, A04207, doi:10.1029/2006JA011993.

Thorne, R. M., et al. (2013), Rapid local acceleration of relativistic radiation-belt electrons by magnetospheric chorus, *Nature*, *504*, 411–414, doi:10.1038/nature12889.

Turner, D. L., Y. Y. Shprits, M. Hartinger, and V. Angelopoulos (2012), Explaining sudden losses of outer radiation belt electrons during geomagnetic storms, *Nat. Phys.*, *8*, 202–212, doi:10.1038/nphys2185.

Ukhorskiy, A. Y., M. I. Sitnov, K. Takahasi, and B. J. Anderson (2009), Radial transport of radiation belt electrons due to stormtime Pc5 waves, *Ann. Geophys.*, *27*, 2173–2181, doi:10.5194/angeo-27-2173-2009.

West, H. I., Jr., R. M. Buck, and J. R. Walton (1973), Electron pitch angle distributions throughout the magnetosphere as observed on Ogo 5, *J. Geophys. Res.*, *78*, 1064–1081, doi:10.1029/JA078i007p01064.

Xiao, F., C. Yang, Zhenpeng S., Q. Zhou, Z. He, Y. He, D. N. Baker, H. E. Spence, H. O. Funsten, and J. B. Blake (2015), Wave-driven butterfly distribution of Van Allen belt relativistic electrons, *Nat. Commun.*, *6*, 8590, doi:10.1038/ncomms9590.

Zhao, H., et al. (2014a), Peculiar pitch angle distribution of relativistic electrons in the inner radiation belt and slot region, *Geophys. Res. Lett.*, *41*, 2250–2257, doi:10.1002/2014GL059725.

Zhao, H., et al. (2014b), Characteristics of pitch angle distributions of hundreds of keV electrons in the slot region and inner radiation belt, *J. Geophys. Res. Space Physics*, *119*, 9543–9557, doi:10.1002/2014JA020386.